Picosecond time-resolved luminescence studies of surface and bulk recombination processes in InP

Y. Rosenwaks and Yoram Shapira
Department of Electrical Engineering–Physical Electronics, Faculty of Engineering, Tel Aviv University, Ramat Aviv, Tel Aviv 69978, Israel

D. Huppert
Beverly and Raymond Faculty of Exact Sciences, School of Chemistry, Tel Aviv University, Raman Aviv, Tel Aviv 69978, Israel
(Received 10 October 1991)

Recombination processes in InP have been studied using picosecond-time-resolved photoluminescence (PL). The technique makes it possible to measure the intrinsic surface recombination velocity (SRV) and the bulk lifetime τ directly and independently. The results show that both p- and n-type InP(110) etched surfaces have similarly low SRV, contrary to commonly accepted values. Moreover, it is found that n-type InP is distinguished by a very long nonradiative lifetime τ_{nr} (320 ns) and the bulk recombination process is mainly radiative. On the other hand, the τ_{nr} of p-type InP is very small (≤ 33 ns), apparently due to a high concentration of deep traps, and nonradiative bulk recombination is dominant. These results are discussed in view of other measurements and models. The SRV of metal/InP interfaces shows a strong dependence on the reactivity of the metal-semiconductor anion pair, which resembles the dependence found for the Schottky-barrier height at these interfaces. These measurements are compared to results also obtained in this work for UHV-cleaved surfaces.

I. INTRODUCTION

In the last decade there has been considerable interest in InP both as a prototypical III-V compound suitable for basic studies, and as a potential candidate for a variety of electronic and optoelectronic devices. InP plays a crucial role in the high performance of $Ga_{1-x}In_xAs_{1-y}P_y$ (Ref. 1) and $Ga_{1-x}In_xAs$ (Ref. 2) avalanche photodiodes, lasers, and light-emitting diodes. It also has important applications in integrated electro-optics and in a variety of microwave and high-speed digital circuits[3] due to its high-saturation drift velocity and high mobility. Recently, InP-based solar cells have been recognized as having great potential for space applications because of their extraordinary radiation resistance.[4] Nonradiative recombination of carriers plays a vital role in the performance of these devices. Nonradiative recombination occurs mainly through near-midgap defect levels. These defects may be present in the volume (bulk) of the crystal or at its surface. Bulk recombination is quantified by the excess carrier lifetime τ, while recombination at the surface by a parameter called surface recombination velocity (SRV).

In spite of the numerous applications of InP, very little has been done regarding direct measurement of its τ and SRV. The data on both parameters are limited and sometimes inconsistent. In a recent review article[5] it has been shown that the lifetimes measured on n-type crystals are in the range of 1–3000 ns, depending on crystal quality and growth methods. On the other hand, there is only a single report on lifetime measurements (200 ns) in p-type InP.[6] The low SRV of n-type InP has been observed by Casey and Buehler[7] through steady-state photoluminescence (PL) measurements. In addition, they found that the PL intensity of p-type InP was more than two orders of magnitude lower than in n-type InP, similar to the value obtained for GaAs. This led many researchers to the conclusion that the SRV of p-type InP was very high—around 10^6 cm/s. Hoffman, Gerritsen, and Nurmikko[8] conducted a direct measurement of intrinsic SRV of InP by means of transient diffraction from free-carrier plasma gratings generated by picosecond laser pulses. They measured SRV values of 2×10^4 and 1.5×10^5 cm/s for n- and p-type InP, respectively. Since then, there has been only a single other report[9] describing direct SRV measurements on InP.

Obviously, much more data are needed on the SRV and τ of InP. We report here the results of an extensive and systematic study of surface and bulk recombination processes in both n- and p-type InP. The measurements were based on a time-resolved PL technique, previously developed by our group.[10] The method (described in more detail in Sec. II) has been applied to CdS and CdSe (Refs. 11 and 12) and recently in InP.[13] Its great advantage is the possibility of unambiguous determination of both SRV and τ *under flat-band conditions.*

The method for extracting the SRV and τ values from the time-resolved PL measurement is briefly described in Sec. II. The experimental techniques we have used are described in Sec. III. Our results are presented and discussed in Sec. IV, which is divided into four subsections, each dealing with a different subject. Section IV A describes SRV and τ measurements on etched n-type InP (110). It is found that the radiative process is the dominant bulk-recombination mechanism. Section IV B describes similar measurements conducted on p-type InP. It is found that its intrinsic SRV value is low, similar to the value obtained for n-type InP, but its bulk lifetime is nearly two orders of magnitude smaller and is dominated

by the nonradiative recombination process. SRV measurements at (n-InP type)/ metal interfaces are presented in Sec. IV C. Section IV D describes SRV measurements of n-type InP performed under ultrahigh vacuum (UHV) conditions. The results are summarized in Sec. V.

II. SRV AND τ MEASUREMENT METHODS

SRV and τ are typically determined by measuring decay times of excess carriers generated by optical means. These decay times depend on several parameters: (1) Intensity and penetration depth of the exciting light, (2) diffusion of excess carriers, (3) radiative and nonradiative bulk and surface recombination, (4) reabsorption of emitted photoluminescence as a result of the radiative recombination process, and (5) surface band bending.

We have developed a method for extracting SRV and τ which takes into account the above factors.[10] The method is based on comparing PL decay curves with experimental results. The normalized, time-dependent PL intensity, $I(t)$, is calculated by

$$I(t)=\int_0^\infty \Delta n^2(x,t)\exp(-\alpha_L x)dx \ , \tag{1}$$

where $\Delta n(x,t)$ is the excess carrier concentration and α_L is the absorption coefficient for the gap-luminescence wavelength. The value of $\Delta n(x,t)$ is calculated using the ambipolar diffusion equation:[14]

$$\frac{\partial \Delta n(x,t)}{\partial t}=D^*\frac{\partial^2 \Delta n(x,t)}{\partial x^2}+g(x,t)-\frac{\Delta n(x,t)}{\tau} \tag{2}$$

with the boundary conditions

$$\left.\frac{\partial \Delta n(x,t)}{\partial x}\right|_{x=0}=\frac{S_0}{D^*}\Delta n(x=0,t) \ , \tag{3}$$

$$\Delta n(x\rightarrow\infty t)=0 \ , \quad \Delta n(x,t=0)=0 \ . \tag{4}$$

D^* is the ambipolar diffusion constant, $g(x,t)$ the laser-generation function, τ the effective bulk lifetime, and S_0 the ambipolar or intrinsic SRV, which will be defined later. The use of Eq. (2) is valid only under high-excitation conditions, as we have shown in the past.[10] Under such conditions, D^* and τ are independent of the excess carrier concentration and the bands near the surface are flat. Vaitkus[15] has derived an analytical solution for Eq. (2) for the case of a δ-function excitation pulse, where $g(x,t)$ is given by $g(x,t)=\alpha\exp(-\alpha x)\delta(t)$, where α is the absorption coefficient for the excitation wavelength. Vaitkus's solution cannot be used when the excitation level decreases and the dependence of D^* and τ on the excess carrier concentration cannot be neglected anymore. In addition, it is not suitable when radiative recombination has to be taken into account. In such cases we have used a numerical algorithm to solve the ambipolar diffusion equation. In both cases the PL intensity was calculated according to Eq. (1) and then convoluted with the experimental laser-pulse instrumental response (recorded before each PL measurement) in order to fit the experimental PL decay curve.

It is generally accepted that the surface recombination rate R_s can be described by the Shockley-Read-Hall statistics as

$$R_s=\sum_j N_{sj}\frac{\sigma_n^j\sigma_p^j v_n v_p(p_s n_s-n_i^2)}{\sigma_n^i v_n(n_s+n_T^j)+\sigma_p^j v_p(p_s+p_T^j)} \ . \tag{5}$$

Here N_{sj} is the density per unit area of surface states at an energy level j, $\sigma_n^j(\sigma_p^j)$ is the capture cross section for electrons (holes) at surface state j, $v_n(v_p)$ is the electron (hole) thermal velocity, $n_T^j(p_T^j)$ is the electron (hole) density in the conduction (valence) band if the quasi-Fermi levels are located at the surface-state energy j [see Eq (17)], and $n_s(p_s)$ is the surface density of electrons (holes). If for simplicity we assume that the recombination takes place mainly through centers located at midgap energy (in fact, such centers are the most effective) and that no surface space-charge region exists ("flat-bands" conditions—$n_s=p_s$), then the SRV defined as $v_{SR}=R_s/\Delta n$, can be written as

$$v_{SR}\equiv S_0=N_s\frac{\sigma_n\sigma_p v_n v_p}{\sigma_n v_n+\sigma_p v_p}=\frac{S_{0n}S_{0p}}{S_{0n}+S_{0p}} \ , \tag{6}$$

where S_{0n} (S_{0p}) are the individual surface recombination velocities of electrons (holes) under flat-bands conditions, defined (e.g., for holes) as $S_{0p}=\sigma_p v_p N_s$. S_0 is called the "intrinsic" or "ambipolar" surface recombination velocity. In the derivation of Eq. (6) it was also assumed that $n_s=p_s\gg n_T, p_T$, an assumption that is valid for InP even under moderate excitation conditions. Rzhanov and Arkhipura[16] have derived an expression identical to Eq. (6) for the case of high-excitation (injection) conditions in the presence of a space-charge region. Such a situation also exists under our experimental conditions.

III. EXPERIMENT

The samples used were n- and p-type InP with either (110) or (100) surface orientation, supplied by MCP Electronic Materials (Alperton, Middlesex, England). They had bulk-carrier densities of $n_0=4.85\times10^{16}$ cm^{-3} (Si-doped), $p_0=4\times10^{15}$ cm^{-3}, $p_0=4.65\times10^{17}$ cm^{-3} (Zn doped) for (110)-oriented surfaces, and $p_0=5\times10^{16}$ cm^{-3} (Zn doped) for (100)-oriented surfaces. The samples were etched by aqua regia, and atomically clean and visually flat (110) surfaces were achieved by cleavage of bars in an UHV chamber at pressures below 1×10^{-10} Torr.

We have set up and used two different systems for time-resolved PL measurements. The first one is schematically shown in Fig. 1. It is based on a cw mode-locked Nd/YAG (Cherent Antares) pumped cavity dumped dye laser (Coherent Inc. 702) providing high repetition rate of short pulses (1 ps full width at half maximum). The laser was operated at a wavelength of 595 nm, and at a repetition rate of 380 kHz. The beam was focused onto a spot size approximately 1 mm in diameter on the crystal surface, creating an initial electron-hole concentration of about 5×10^{18} cm^{-3} (based on $\alpha=5.3\times10^4$ cm^{-1} at 595-nm wavelength). The crystal band-gap luminescence (at 925 nm) was collected by a combination of a monochromator, a cooled MCP (multichannel plate) photomultiplier (Hamamatsu-R1564U-05 s-1 photocathode) and a time-correlated single-photon-

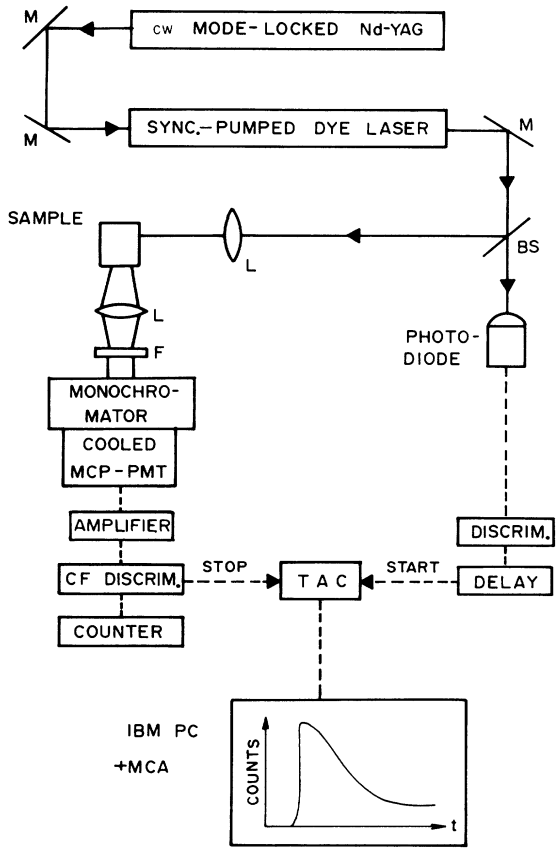

FIG. 1. The main time resolved photoluminescence system. *M* denotes mirrors; BS denotes beamsplitter; *L* denotes lens; *F* denotes filters.

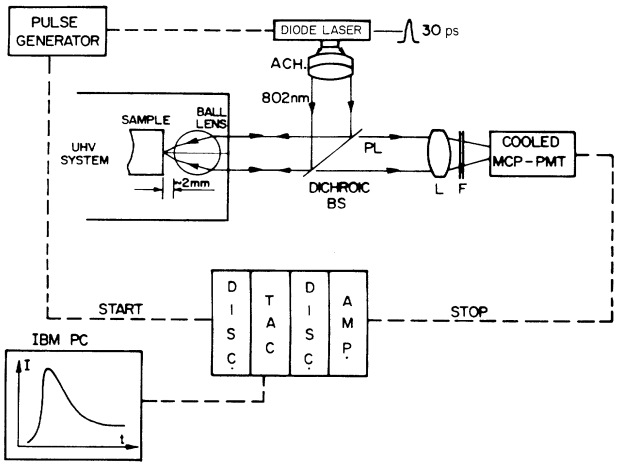

FIG. 2. The time-resolved photoluminescence system used for the measurements under UHV conditions. ACH denotes Achromat lens; *L* denotes lens; *F* denotes filters; BS denotes beamsplitter.

counting (TCSPC) system. The TCSPC is based on a modified Tennelec constant fraction (CF) discriminator (TC454), Tennelec TAC 864 and an IBM PC-based multi-channel analyzer (Nucleous PCA-II). The overall instrumental time response (full width at half maximum) was about 50 ps. The laser repetition rate and spot size were carefully chosen in order to prevent crystal heating and surface damage and to ensure a stable signal during the entire measurement time.

In order to conduct the PL experiments inside the UHV chamber we have used the system shown schematically in Fig. 2. The excitation source is an ultrafast diode laser (Opto-Electronics Inc., model PLS10) providing short pulses (35 ps full width at half maximum) at a wavelength of 802 nm, and a maximum peak power of 680 mW. The laser is driven by a control unit (Opto-Electronics Inc., LCU10) which features a pretrigger output with less than 5-ps jitter and a variable repetition rate up to 30 kHz. The diode laser pulse is reflected off a dichroic beam spitter and focused by a ball lens (*f* number of 0.69) which is inside the UHV chamber, onto a sample surface. The crystal luminescence is collected by the same lens and is transmitted through the beam splitter to the photomultiplier. The reflected and scattered light are blocked first by the dichroic beam splitter, then by two colored glass filters (Schott RG850) and by a 920-nm interference filter. The laser is operated at 20 kHz and the luminescence collection rate is kept below 1000 counts per second. This requires a typical measurement time of 15 min in order to collect about 1000 counts at the peak channel.

InP-metal interfaces were formed in a high vacuum system (base pressure below 1×10^{-6} Torr) equipped with a quartz-crystal thickness monitor. The PL of the crystals was recorded in air just before each metal evaporation (in order to verify the low-SRV value obtained by the etching process) and soon afterwards. There was no marked influence of the air exposure time on the SRV.

IV. RESULTS AND DISCUSSION

A. *n*-type InP

Figure 3 shows I_{PL} measured as a function of the exciting laser pulse intensity for two different *n*-type InP samples with $n_1=5\times10^{16}$ cm^{-3} (full squares) and $n_2=8\times10^{17}$ cm^{-3} (open squares). This measurement is carried out in order to verify the high-excitation conditions.

The normalized photoluminescence intensity I_{PL} can be written as

$$I_{PL}=(n_0+\Delta n)(p_0+\Delta p)\ , \tag{7}$$

where $n_0(p_0)$ is the equilibrium concentration of majority (minority) carriers. Under high excitation ($\Delta n=\Delta p \gg p_0$ for *n*-type sample)

$$I_{PL}=(n_0+\Delta n)\Delta n\ . \tag{8}$$

The PL intensity of the two samples is normalized so that it has the same value for a laser pulse intensity of 0.7 on our scale. The highest intensity corresponds to ~5 MW/cm^2 (peak power) and lower-intensities were obtained using calibrated neutral-density filters. The lines represent the calculated PL intensity according to Eq. (8).

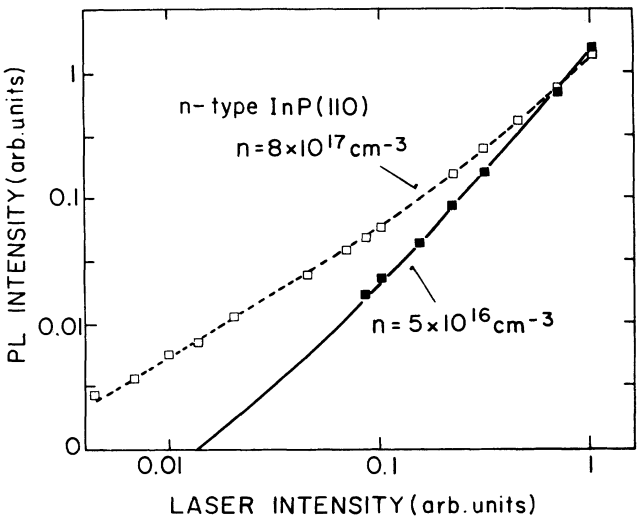

FIG. 3. Photoluminescence intensity as a function of the exciting-laser intensity. Open (full) squares represent the experimental results for the strongly (weakly) doped sample, and the curves are calculated according to Eq. (8).

I_{PL} is quadratic with the laser-pulse intensity for the weakly doped crystal. Linear regression analysis yields a slope of ~ 1.93 corresponding to $\Delta n_0 = 1.5\times 10^{18}$ cm^{-3}, where Δn_0 is the initial excess-carrier concentration produced by the unattenuated laser pulse. This shows that high-excitation conditions are satisfied for the weakly doped crystal.

Figure 4 shows the experimental (dotted curve) and calculated (solid curve) PL decay curves for the weakly doped crystal ($n_0 = 5\times 10^{16}$ cm^{-3}) measured on the 100-ns time scale. The parameters used for obtaining the theoretical curve were $D^* = 4.5$ cm^2/s, $\alpha = 5.3\times 10^4$ cm^{-1}, $\alpha_L = 1\times 10^3$ cm^{-1}, $v_{SR} = 250$ cm/s, and $\tau = 320$ ns. The values of D^*, α, and α_L were taken from the literature.[5] SRV and τ were the adjustable parameters in the

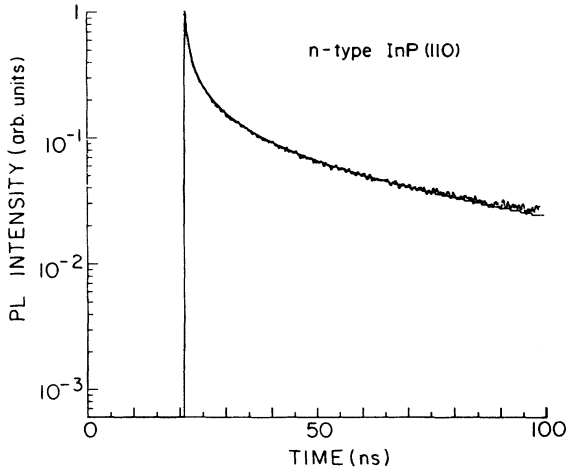

FIG. 4. Experimental (dotted curve) and calculated (solid curve) photoluminescence decay curves for etched n-type InP ($n = 5\times 10^{16}$ cm^{-3}) measured on a 100-ns time scale.

fitting procedure. Such low SRV values were predicted in the past[7,8] but to the best of our knowledge this is their first direct measurement. The value of τ agrees with most of the reported values for bulk material which are between 100 and 425 ns.[5] In general, the PL has been found to decay faster with increasing laser intensity. This may be due to two different reasons. (a) The dependence of the ambipolar diffusion constant on the excess carrier concentration. Under high-excitation conditions $D^* \cong 2D_P$ (Ref. 15) where D_P is the hole diffusion constant. When the laser intensity is lowered, D^* decreases, reaching D_P under low-excitation conditions. In our experiments, $n_0 \le \Delta n \le 100 n_0$ (at $x = 0$ and $t = 0$, for $n_0 = 5\times 10^{16}$ cm^{-3}), so for the lowest laser intensity ($\Delta n \sim n_0$), $D^* \sim 1.5 D_P$. This small change in D^* is insufficient to account for the observed changes in the PL decay curves. (b) Radiative bulk recombination. The radiative bulk lifetime τ_r is given for the general case by[17]

$$\frac{1}{\tau_r} = B(p_0+\Delta p)(n_0+\Delta n)/\Delta n \ , \tag{9}$$

where B is the radiative rate constant. Under moderate excitation conditions and for n-type samples, Eq. (9) simplifies to

$$\tau_r = \frac{1}{B(\Delta n + n_0)} \ . \tag{10}$$

Hence τ_r decreases with increasing Δn, which is in agreement with our experimental results. In order to calculate Δn, taking into account the effect of the radiative recombination, we have used a numerical algorithm to solve the ambipolar diffusion equation. The equation is identical to Eq. (2) except for τ which depends on Δn according to

$$\tau = \frac{\tau_r \tau_{nr}}{\tau_r + \tau_{nr}} = \frac{\tau_{nr}}{1+\tau_{nr} B(\Delta n + n_0)} \ , \tag{11}$$

where τ_{nr} is the nonradiative (Shockley-Read) bulk lifetime. Figure 5 shows experimental (dotted curves) and calculated (solid curves) PL decay curves for the n-type InP crystal measured under different excitation intensities, I, given in Table I. Curve a corresponds to the unattenuated laser beam with intensity $I = I_0$, producing an initial (at $x = 0$ and $t = 0$) excess carrier concentration $\Delta n_0 = 3.3\times 10^{18}$ cm^{-3}. The values of Δn_0, B, and τ_{nr} were chosen to obtain a best fit of the calculated to the

TABLE I. A comparison between the experimental laser attenuation (I/I_0) and the corresponding normalized excess-carrier concentration ($\Delta n/\Delta n_0$) used for calculating curves (a)–(d), in Fig. 5.

Experimental curve	Relative laser intensity I/I_0	Calculated normalized excess-carrier concentration $\Delta n/\Delta n_0$
(a)	0.05	0.09
(b)	0.10	0.12
(c)	0.25	0.30
(d)	1.00	1.00

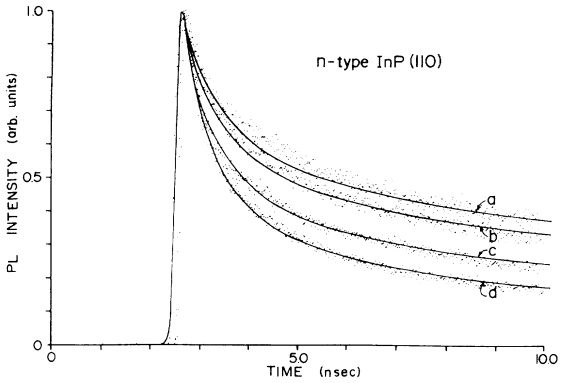

FIG. 5. Experimental (dotted curves) and calculated (solid curves) photoluminescence decay curves for n-type InP ($n=5\times10^{16}$ cm^{-3}) measured under different excitation intensities. Each solid curve was calculated with a different value of excess-carrier concentration Δn given in Table I.

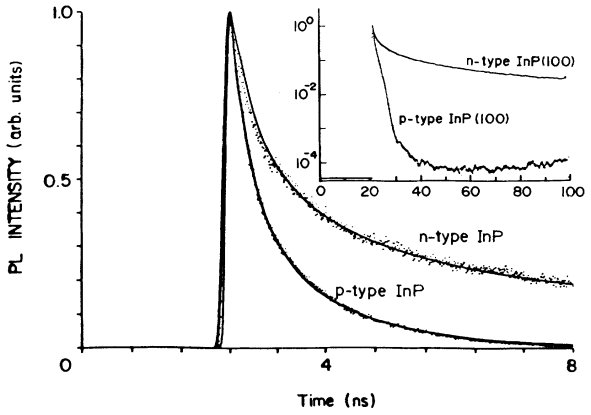

FIG. 6. Experimental (dotted curves) and calculated (solid curves) photoluminescence decay curves for etched p- and n-type InP. The calculated curves were obtained using similar SRV values. The inset shows the decay curves for the same two crystals measured on the 100-ns time scale.

experimental curve. Curves b, c, and d were fitted with the same τ_{nr} and B but with different Δn values given in Table I. The table shows a comparison between the normalized laser intensity I/I_0 and the calculated normalized-excess-carrier concentration ($\Delta n/\Delta n_0$) used for calculating the different curves. I_{PL} was calculated according to

$$I_{PL}=\int_0^\infty\{[n_0+\Delta n(x,t)]\Delta n(x,t)\}\exp(-\alpha_L x)dx \qquad (12)$$

in order to account for the moderate excitation conditions. The correlation between columns 2 and 3 in Table I is reasonable except for the case of curve d. In that case, the dependence of D^* and τ_{nr} on Δn cannot be neglected anymore. The curves were best fitted with $B=3\times10^{-11}$ cm^{3}s^{-1}. In contrast with GaAs, for which the radiative rate constant is well known [around $(1-3)\times10^{-10}$ cm^{3}s^{-1} (Ref. 17)], no information has been found for InP. B is a function of the semiconductor absorption spectrum, so it is assumed that its value for InP is also around 1×10^{-10} cm^{3}s^{-1}. The low value of 3×10^{-11} cm^{3}s^{-1} used in our calculations is probably due to the photon-recycling process. In this process[18] the photoluminescence photons are reabsorbed producing new electron-hole pairs which may again recombine radiatively. Hence the self-absorption process increases τ_r — and reduces B [see Eq. (10)]. In summary, the results show that the bulk recombination process is principally radiative.

B. p-type InP

1. Evidence for low intrinsic SRV

Figure 6 shows experimental (dotted curves) and calculated (solid curves) PL decay curves for n- and p-type InP of similar doping [$(4-5)\times10^{16}$ cm^{-3}]. Both crystal surfaces were identically prepared by aqua regia etching. The parameters used for the calculated solid curves were as follows: $D^*=5$ cm^2/s, $\alpha=5.3\times10^4$ cm^{-1}, and $\alpha_L=1\times10^3$ cm^{-1}, $\tau=320$ and 4 ns for n- and p-type InP, respectively. The most striking thing about this fit is that the SRV for p-type InP was very low (500 cm/s), almost as low as the valued obtained for n-type InP (200 cm/s). It was not possible to fit the curve for p-type InP with higher SRV and τ. The inset shows the experimental decay curves for the same two crystals measured on a 100-ns time scale.

As mentioned in Sec. I, Casey and Buehler and other groups (see Ref. 19, and references therein) reported that the steady-state PL intensity of n-type InP was much higher (more than two orders of magnitude) than that of p-type InP. Our results show that this difference is partly due to different bulk properties while the intrinsic surface recombination velocities are essentially similar. The large difference in τ between the n- and p-type crystals is evident from the inset of Fig. 6. The steady-state PL intensity is actually the area under the PL decay curve when measured on an infinitely long time scale. Hence it is clear that such a difference in τ should have a pronounced effect on the steady-state PL signal. This effect also points to a great advantage of time-resolved PL as a tool for measuring SRV. The method unambiguously determines SRV and τ since each parameter dominates a different part of the decay curve.

Another factor which may decrease the PL intensity is the presence of a surface depletion layer. Wittry and Kyser[20] showed that carriers generated in such a surface layer do not recombine radiatively and designated this region as a "dead layer." Ando, Yamaoto, and Yamaguchi[21] calculated the PL intensity as a function of surface potential and found that the PL intensity decreases only by a factor of 2 when the band bending at the surface is increased from 0.1 to 0.8 V. However, band bending can affect the value of the PL intensity through the so-called effective-SRV value.

An expression for the effective SRV in the presence of a depletion layer at the semiconductor surface has been

presented by Grove.[22] For a p-type semiconductor it takes the form

$$S_n = S_{0n}\frac{N_A}{n_s + p_s + 2n_i}\ , \tag{13}$$

where S_n is the effective-electron SRV evaluated at the depletion layer edge, N_A is the semiconductor dopant concentration, and n_i is the intrinsic carrier concentration. The quantity S_n may be interpreted as the speed at which the electrons flow from the neutral bulk into the space-charge layer where they recombine nonradiatively at an intrinsic velocity S_{0n}. Steady-state PL studies generally refer to this "effective" SRV rather than to the intrinsic-value S_{0n}, for two reasons. First these experiments are conducted under low-excitation conditions and, hence, in the presence of a surface depletion layer. Secondly, no radiative recombination takes place in the space-charge region.

A careful examination of Eq. (13) shows that under low-excitation conditions and in the presence of a surface-depletion region (i.e, $n_s \ll N_A$) S_n is always greater than S_{0n} and the ratio between the two is proportional to the crystal doping. This is the reason the effective SRV of p-type InP is high. In n-type InP, on the other hand, the surface band bending is very low [<0.1 V (Ref. 23)], so even under low-excitation conditions $n_s \sim N_D$ (the dopant concentration) and $S_p \sim S_{0p}$. In conclusion, the low PL efficiency of p-type InP is due to small τ and a wide surface-depletion region giving rise to a high effective SRV.

In order to check whether the measured SRV indeed reflect an intrinsic material property and are not doping-level dependent, we performed PL measurements on crystals with various doping concentrations. The results are shown in Fig. 7. The three crystals measured had doping concentrations of (a) 4×10^{15} cm^{-3}, (b) $4-5\times10^{16}$ cm^{-3}, and (c) $4-5\times10^{17}$ cm^{-3}. The fit to the highly doped crystal (c) is fair because the excess carrier concentration

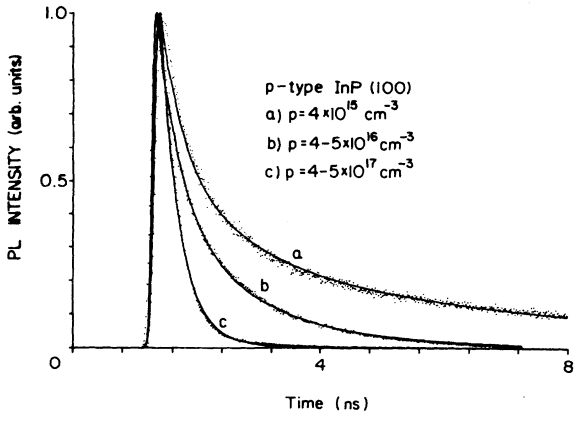

FIG. 7. Experimental (dotted curves) and calculated (solid curves) photoluminescence decay curves for three p-type InP(100) wafers with different doping concentrations. All the solid curves were calculated with the same SRV (500 cm/s) but with different τ given in the text.

was not much higher than the bulk doping, especially a few ns after the laser pulse (in the tail of the curve). In this case, the high-excitation conditions are not satisfied and the dependence of D^* and τ on Δp must be taken into account. All the solid curves were calculated using *the same* SRV (500 cm/s) but with different τ of 33, 4, and 0.85 ns for a, b, and c, respectively. (The values of D, α, and α_L were the same as in Fig. 6.) The dependence of τ on the doping level can be explained by the expressions for τ_{p0} and τ_{n0}, the well-known minority carrier lifetimes in extrinsic materials, given by

$$\tau_{p0} = \frac{1}{\sigma_P v_p N_B}\ ,\quad \tau_{n0} = \frac{1}{\sigma_n v_n N_B}\ , \tag{14}$$

where N_B is the bulk trap concentration.

Under high-excitation conditions $\tau \approx \tau_{n0} + \tau_{p0}$ and the latter are inversely proportional to N_B. The latter increases with increasing doping level, thus reducing τ_{nr}.

Our hypothesis about the low SRV of p-type InP can also be checked by trying to obtain higher SRV by contaminating the crystal surface. It was found that the SRV can be controlled over the entire range between 500 and 10^6 cm/s by depositing different metals on the crystal surface. This will be described in detail for n-type InP in Sec. IV B.

2. *Excitation-intensity dependence of bulk recombination lifetime of p-type InP: Comparison with n-type InP.*

Figure 8 shows PL decay curves measured for a medium doped ($p_0 = 5\times10^{16}$ cm^{-3}) p-type InP sample at three different laser intensities [(a) I_L, (b) 0.7 I_L, (c) 0.2 I_L]. Comparing this figure with Fig. 5 two major differences are immediately apparent: (a) the effective PL decay times for the p-type crystals are much shorter (nearly two orders of magnitude) than the ones obtained for the n-type InP crystals; (b) the effective PL decay rate decreases with increasing laser power, in contrast with the results obtained for the n-type crystals. The decrease in the PL decay time can be explained by the dependence of τ_{nr} on the excess-carrier concentration Δp. τ_{nr} was expressed by Shockley and Read[24] as

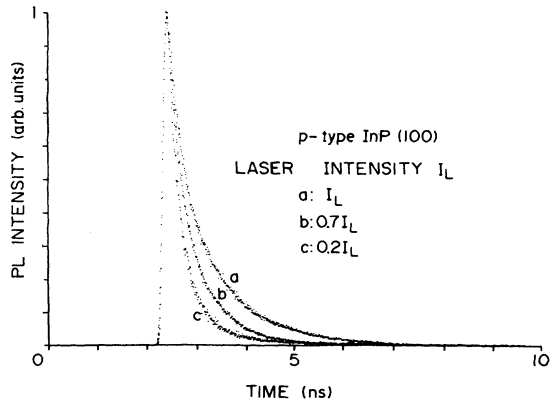

FIG. 8. Photoluminescence decay curves of p-type InP(100) measured at three different laser intensities: (a) I_L; (b) 0.7 I_L; (c) 0.2 I_L.

$$\tau_{nr}=\frac{\tau_{p0}(n_0+n_T+\Delta p)+\tau_{n0}(p_0+p_T+\Delta p)}{p_0+n_0+\Delta p} . \quad (15)$$

Considering p-type crystals and using p_T and n_T values which satisfy $n_T \ll p_T \ll p_0$, Δp (moderate- and high-excitation conditions) we obtain

$$\tau_{nr}\simeq\frac{\tau_{p0}\Delta p+\tau_{n0}(p_0+\Delta p)}{p_0+\Delta p}=\frac{\tau_{p0}}{p_0/\Delta p+1}+\tau_{n0} . \quad (16)$$

Equation (16) shows that by increasing Δp — by using higher laser power—τ_{nr} increases and, as a result, the PL decay rate decreases. This is in qualitative agreement with our experimental results shown in Fig. 8.

Figure 9 shows a plot of τ_{nr} as a function of Δp [calculated using Eq. (15)] for three doping levels: (a) 5×10^{15} cm^{-3}, (b) 5×10^{16} cm^{-3}, (c) 5×10^{17} cm^{-3}. The values of τ_{n0} and τ_{p0} were taken as 0.85 and 30 ns, respectively, and $p_T=5\times10^{14}$ cm^{-3}. p_T and n_T are defined as

$$p_T=n_i\exp\left[\frac{E_i-E_T}{kT}\right] ; \quad n_T=n_i\exp\left[\frac{E_T-E_i}{kT}\right] , \quad (17)$$

where E_i is the intrinsic Fermi level, and E_T is the trap energy level. Thus a large $p_T(n_T)$ value implies that the trap energy is closer to the valence (conduction) band. If $p_T=5\times10^{14}$ cm^{-3}, then according to Eq. (17) $E_i-E_T\cong0.46$ eV. Figure 9 and Eq. (16) also show that under high-excitation conditions ($\Delta p \gg p_0$) $\tau_{nr}\approx\tau_{n0}+\tau_{p0}$ and thus it is independent of Δp, which justifies the use of the Vaitkus solution as discussed in Sec. II. Figure 9 shows that τ_{nr} of the low-doped sample is almost independent of the laser power at the intensities used in our experiments (i.e., laser intensities that produce 5×10^{18} cm$^{-3}\geq\Delta p\geq5\times10^{16}$ cm^{-3}). This is demonstrated in Fig. 10 which shows two experimental and calculated (solid curves) PL decay curves for low-doped ($p_0=4$–5×10^{15} cm^{-3}) p-type InP measured at two different laser intensities. The lower curve was measured when the beam was attenuated by a factor of 4 relative to the upper one. Fitting the curves using the Vaitkus solution yielded $\tau=33$ and 30 ns for the upper and lower curves, respectively. The difference from Fig. 8 is immediately noted. First, the lifetime is longer and in addition it is weakly dependent on Δp in agreement with Eq. (15), Fig. 10, and the above discussion.

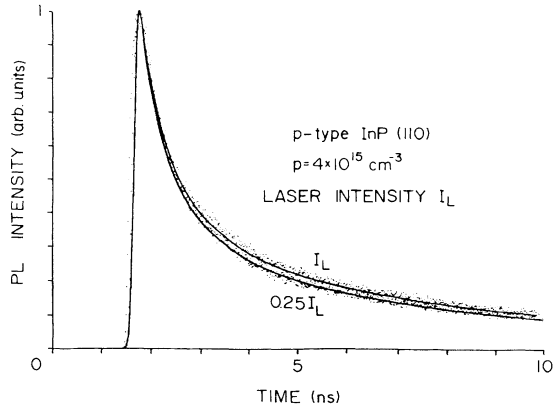

FIG. 10. Experimental (dotted curves) and calculated (solid curves) photoluminescence decay curves for low-doped ($p=3$–5×10^{15} cm^{-3}) InP measured at two different laser intensities: (a) at a laser intensity I_L, $\tau=33$ ns, (b) at a laser intensity $I_L/4$, $\tau=30$ ns.

We will now discuss the reasons for the much longer τ of n-type InP. The main reason may be the bulk-trap energy position in the gap. It is reasonable to assume that the recombination process in n-type samples is carried out mainly through shallower traps than in the p-type samples. This is because the recombination cross section (σ) is much smaller for shallower traps. Figure 11 shows

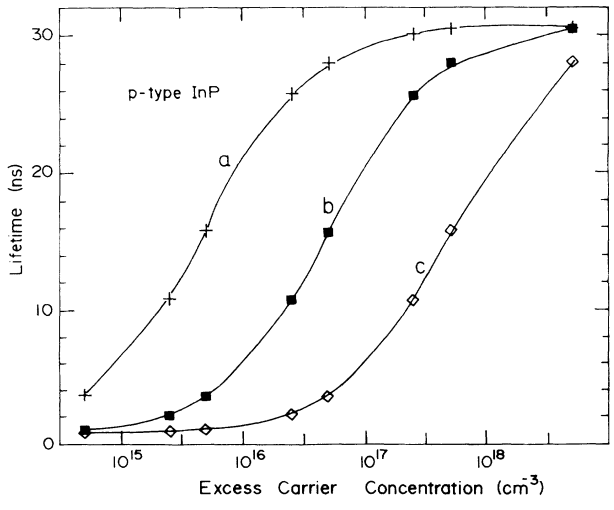

FIG. 9. The nonradiative lifetime (τ_{nr}) as a function of excess-carrier concentration for p-type InP, calculated according to Eq. (14) for three different doping concentrations: (a) 5×10^{15} cm^{-3}; (b) 5×10^{16} cm^{-3}, (c) 5×10^{17} cm^{-3}, and for $p_T=5\times10^{14}$ cm^{-3}.

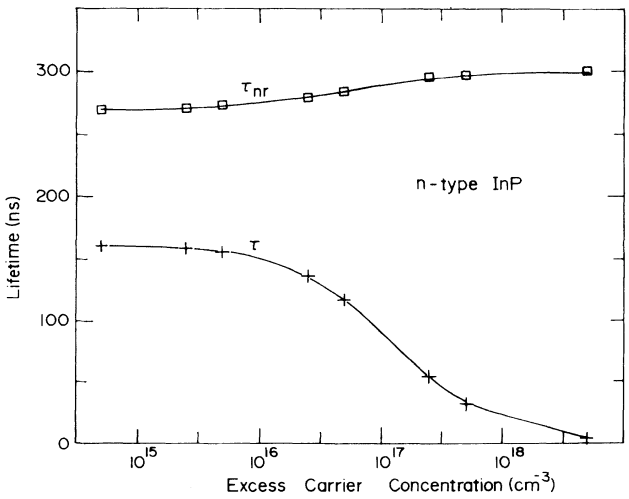

FIG. 11. The nonradiative $-\tau_{nr}$ and the total $-\tau$ lifetimes as a function of excess-carrier concentration for n-type InP. The calculations were based on $n_1=3\times10^{16}$ cm^{-3}, $n_0=5\times10^{16}$ cm^{-3}, and $\tau_{n0}=\tau_{p0}=150$ ns, and $B=5\times10^{-11}$ cm^3 s^{-1}.

τ_{nr} and τ as a function of Δp for n-type InP. The calculation was based on Eq. (14) with $n_T=3\times10^{16}$ cm^{-3}, $n_0=5\times10^{16}$ cm^{-3}, and $\tau_{n0}=\tau_{p0}=150$ ns. τ_{nr} depends more weakly on Δp in comparison with p-type samples (see Fig. 9). τ was calculated according to

$$\frac{1}{\tau}=\frac{1}{\tau_{nr}}+\frac{1}{\tau_r}\ , \tag{18}$$

where τ_{nr} and τ_r were calculated according to Eqs. (15) and (10), respectively. Figure 12 shows the results of similar calculations for p-type InP. The difference between the n- and p-type samples is clearly seen. For n-type InP, $\tau_r \gg \tau_{nr}$, hence the recombination is dominated by the radiative (bimolecular) process and τ decreases with increasing Δp. For p-type InP, on the other hand, τ_{nr} (p-type InP)$\approx 0.01\tau_{nr}$ (n-type InP), the recombination is mainly nonradiative, and as a result τ increases with increasing Δp up to $\Delta p \sim 1\times10^{18}$ cm^{-3}. The difference in the nonradiative lifetimes is probably due to deeper traps present in p-type samples. Such traps have a much higher cross section for electron-hole recombination, thus decreasing τ_{n0} and τ_{p0} according to Eq. (14). The deeper traps also decrease the values of p_T and n_T [see Eq. (17)] and can account for the weaker dependence of τ_{nr} on Δp found in n-type samples

C. Surface recombination velocity measurements at InP interfaces

Figure 13 shows experimental and calculated PL decay curves for n-type InP ($n=5\times10^{16}$ cm^{-3}) before and after deposition of several metals. All the solid curves were calculated with the same parameters (D^*, α, α_L, and τ) used in Fig. 4, so a faster decay indicates a higher SRV due to the metal interfaces.

Figure 14 shows the measured SRV at the different interfaces as a function of ΔH_R—the heat of reaction of each metal phosphide. The values of ΔH_R were calculated per metal atom M for the reaction:

$$M+(y/x)\mathrm{InP}\rightarrow(1/x)M_xP_y+(y/x)\mathrm{In}\ , \tag{19}$$

using the heats of formation ΔH_f (Ref. 25) of the different metal phosphides. Although individual bond energies are not known for many atomic pairs, the sum of bond energies for a given compound contributes directly to the ΔH_R for that compound. For Cr and Cu the choice of the correct phosphide is unclear, so ΔH_R was calculated by averaging the values for the different phosphide compounds as an attempt to obtain a representative value.[26] A greater ΔH_R means a higher barrier for the chemical reaction and thus a less reactive interface

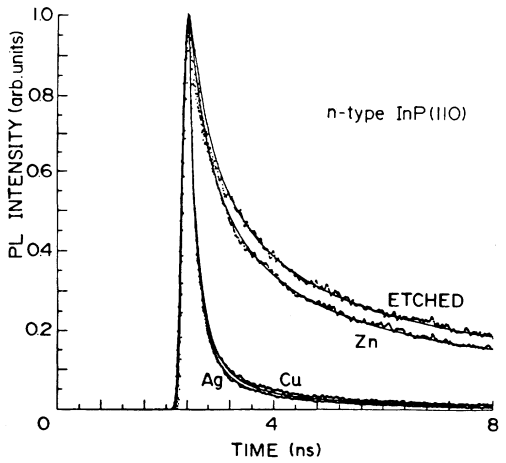

FIG. 13. Experimental (dotted curves) and calculated (solid curves) photoluminescence decay curves for etched n-type InP ($N=5\times10^{16}$cm^{-3}) before and after deposition of several metals.

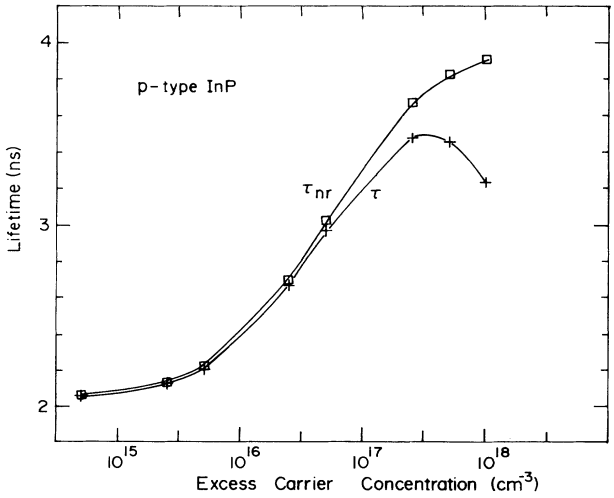

FIG. 12. The nonradiative $-\tau_{nr}$ and total $-\tau$ lifetimes as a function of excess-carrier concentration for p-type InP. The calculations were based on $p=5\times10^{14}$ cm^{-3}, $p_0=5\times10^{16}$ cm^{-3}, $\tau_{n0}=\tau_{p0}=2$ ns, and $B=5\times10^{-11}$ cm^{3}s^{-1}.

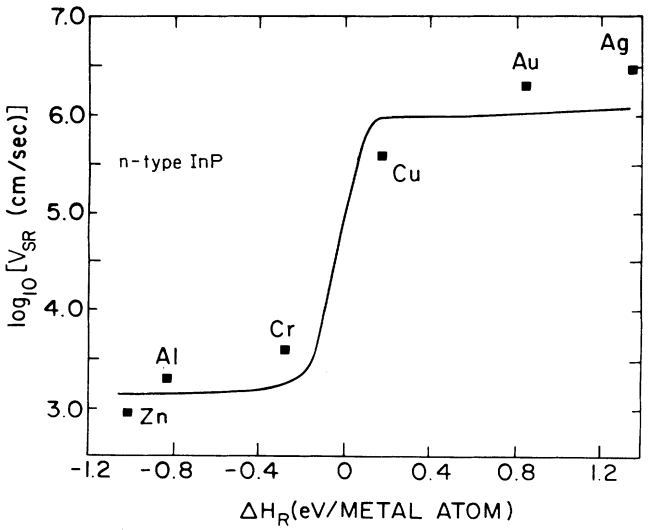

FIG. 14. Surface recombination velocity (SRV) obtained from the simulations of Fig. 13 as a function of ΔH_R — the heat of reaction per metal atom according to Eq. 19.

for the particular metal-semiconductor pair. A similar SRV dependence on ΔH_R was found by us for CdS and CdSe.[11] The explanation given there was that a weak bond at the semiconductor surface would form a surface state close to mid-gap, while a stronger bond would not. The cross section for electron-hole recombination at a surface state i $-\sigma_i$ is higher for surface states closer to midgap. Since SRV is proportional to σ_i, the increase in SRV observed after deposition of less reactive metals is due to the increase in σ_i associated with the midgap surface states formed.

It is very intriguing to consider the similarity between the solid line in Fig. 14 and the dependence of the Schottky-barrier height on ΔH_R. Several authors have reported that reactive (unreactive) metals form low (high) barriers on n-type InP. Williams, Varma, and Montgomery[27] have measured barrier heights of ~ 0.5 eV for Cu, Ag, and Au on etched n-type InP and ~ 0 eV for Al. Hökelek and Robinson[28] have measured barrier heights of 0.37 eV for Al and 0.41 eV for Ag on n-type InP. Brillson[29] has shown that metals which produce Ohmic contacts stabilize the Fermi level the energies less than 0.3 eV below the conduction-band minimum E_c.

Hence it is possible that the *same surface states,* which act as recombination centers and drastically change the SRV, also take part in pinning the surface Fermi level and determine the barrier height. Since it is well known that the barrier height (as well as the SRV) is very sensitive to surface preparation and composition, simultaneous measurements of the Schottky-barrier heights, the interface states' energy positions, and the SRV are needed in order to support this hypothesis.

The surface-state redistribution observed after reactive-metal deposition may also be due to formation of oxides such as Al_2O_3 or ZnO. These oxides have large energy gaps and are unlikely to form gap states. In order to avoid oxide formation, the SRV measurements should be carried out under UHV conditions. Some preliminary work is presented in the next section.

It is generally agreed that SRV at any metal-semiconductor interface is very high, i.e., close to the carrier thermal velocity. This is true if the metal-semiconductor interface is abrupt, in which case carriers reaching the semiconductor interface "see" the infinite density of empty states of the metal and immediately recombine. (In fact, the rate-limiting process is the thermalization of the hot electrons and holes when they reach the metal.) However, since it is now accepted that the semiconductor-reactive metal interface is not abrupt, the probability of excess carrier tunneling into the metal is low and SRV is governed by the semiconductor interface states.

Our results show that the intrinsic SRV at metal-semiconductor interfaces depends on the specific metal and cannot be taken as infinite, as has been assumed by some authors.[22] The results may also suggest a way in which the SRV can be controlled at such contacts, e.g., by using reactive metals as interlayers between the semiconductor and the metal desired to form the contact. However, the Schottky-barrier height of this junction should also be considered.

D. Measurements under UHV conditions

The measurement inside the UHV chamber were carried out using the diode-laser-based system described earlier. The first step was to estimate the excitation conditions, i.e., the initial excess-carrier concentration produced by the diode laser. Figure 15 shows the normalized PL intensity, measured in air, as a function of the diode-laser pulse intensity. The squares represent the experimental results (measured for n-type InP, $n_0 = 5\times 10^{16}$ cm^{-3}) and the solid lines are the PL intensity calculated according to Eq. (8) with three different values of Δn_0. Thus Fig. 15 shows that the measurements are conducted under intermediate ($n_0 \sim \Delta n$) excitation conditions, in contrast with Fig. 3, where $\Delta n \gg n_0$.

Figure 16 shows experimental (dotted curves) and calculated (solid curves) PL decay curves for etched n-type InP (110) excited by the dye laser, $\lambda = 595$ nm, and the diode laser, $\lambda = 802$ nm. The solid curves were calculated using the same D^*, S_0, τ, and α_L, but different α values of 5.3×10^4 and 2×10^4 cm^{-1} for the dye and diode lasers, respectively. Both values are in good agreement with the literature.[30] Figure 16 demonstrates the important role of the excess-carrier diffusion in determining the decay rate of the PL curves. Since the penetration depth of the diode-laser beam is approximately 2.5 times larger than that of the dye laser, the former decreases the concentration gradient of the excess carriers, slows their diffusion to the semiconductor bulk, and yields a slower-decaying PL curve.

Figure 17 shows the PL decay curves obtained after cleaving n-type InP in a vacuum better than 1×10^{-10} Torr. Curve b represents the PL decay curve of the freshly cleaved crystal, $v_{SR} = 6\times 10^3$ cm/s. After evaporation of 0.2 Å of Au, the PL decay rate increased drastically as shown by curve c. The solid line represents the calculation with $v_{SR} = 9\times 10^4$ cm/s. Curve a is the

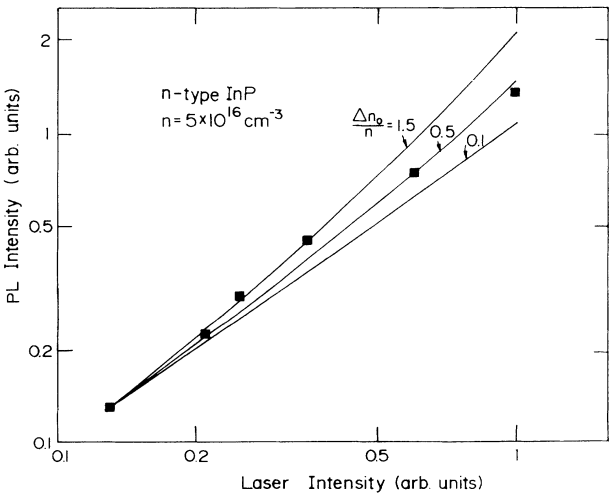

FIG. 15. Photoluminescence intensity as a function of the diode-laser intensity measured for n-type InP ($n = 5\times 10^{16}$cm^{-3}). The solid curves were calculated using Eq. (8) with three different values of Δn_0.

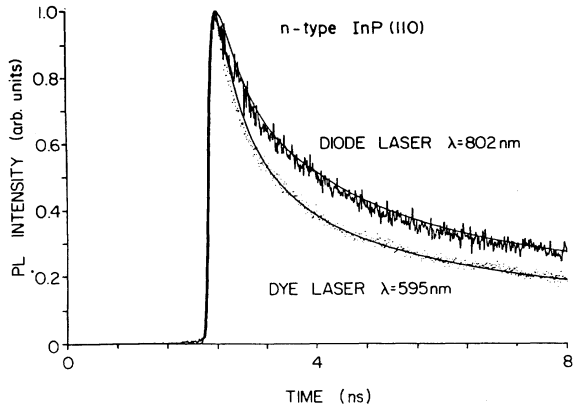

FIG. 16. Experimental (dotted curves) and calculated (solid curves) photoluminescence decay curves for etched n-type InP(110) measured by the dye and diode lasers. The solid curves were calculated using different α values of 5.3×10^4 and 2×10^4 cm^{-1} for the dye- and diode-laser wavelengths, respectively.

result obtained on the etched crystal surface and d the result measured with the dye laser on the etched crystal covered with ~ 15 Å of Au. To the best of our knowledge, this is the first measurement of SRV of cleaved InP(110) under UHV conditions, and the first time-resolved PL measurements in InP under moderate-excitation conditions using a diode-laser source. Such measurements were carried out in the past under low-excitation conditions using high-repetition-rate (50–100 MHz) diode lasers with low peak powers (1–5 mW).[31,32] The results show that SRV of a freshly cleaved crystal is higher than at an etched surface. This may be due to two reasons. First, the cleavage process may have introduced some recombination centers despite the visually smooth mirrorlike surface. The second possibility is that the etching process passivated the crystal surface yielding very low SRV. The SRV of the freshly cleaved crystal remained stable for at least 3 h.

Evaporation of thicker gold layers (up to 10 Å) did not change the luminescence decay curve c. In addition, it is seen that the fit to this curve is fair. These two facts may lead to the conclusion that this measurement was not conducted under flat-band conditions. When the bands near the surface are bent, the photogenerated carriers are separated there and cannot recombine at the surface. Hence, a higher concentration of surface states (as a result of thicker gold layers, for example), will have no measurable effect on the luminescence decay rates. It can be shown that in the case of high SRV ($>10^5$ cm/s) the excess-carrier concentration at the surface decreases by more than one order of magnitude. Thus, based on the diode-laser excitation level estimated earlier ($\Delta n_0 \sim 2.5\times10^{16}$ cm^{-3}) and on the high SRV obtained after the Au deposition, it can be assumed that curve c was measured under low-excitation conditions and hence in the presence of a surface depletion region. In such a case, the ambipolar equation [Eq. (2)] cannot be used to calculate the PL decay curve. Instead, the coupled continuity equations for holes and electrons[14] have to be solved.

Figure 18 shows the PL decay curves obtained after cleaving n-type InP(110) under a pressure of 1×10^{-9} Torr: (b) immediately after cleavage, $v_{SR}=5.0\times10^3$ cm/s; (c) 45 min after cleavage, $v_{SR}=1.4\times10^4$ cm/s; (d) 90 min after cleavage, $v_{SR}=3.0\times10^4$ cm/s. Curve a is the result obtained for the etched crystal. The SRV of the cleaved crystal increased as a function of time even under a pressure of 1×10^{-9} Torr. A residual-gas analysis of the chamber under the pressure showed that the main gases present were H_2O and CO. An estimate of the recombination-centers density caused by these contaminants can be made using the calculated SRV values.

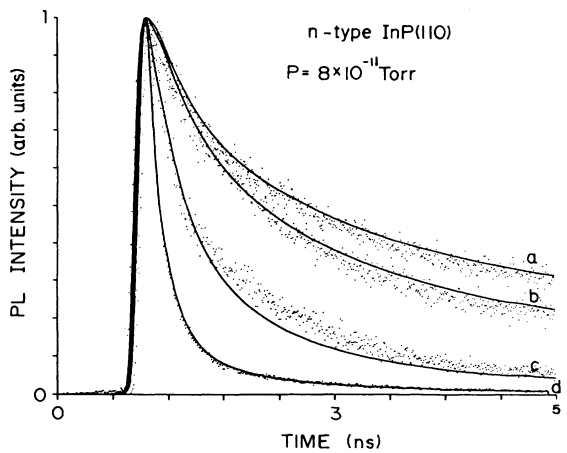

FIG. 17. Experimental and calculated photoluminescence decay curves for cleaved n-type InP(110) under a pressure of $<1\times10^{-10}$ Torr. b, as cleaved ($v_{SR}=6\times10^3$ cm/s); c, after evaporation of 0.2 Å of Au ($v_{SR}=9\times10^4$ cm/s), and the etched (110) +15Å of Au (d) are measured by the dye laser. The etched (110) surface decay curve a is shown for comparison.

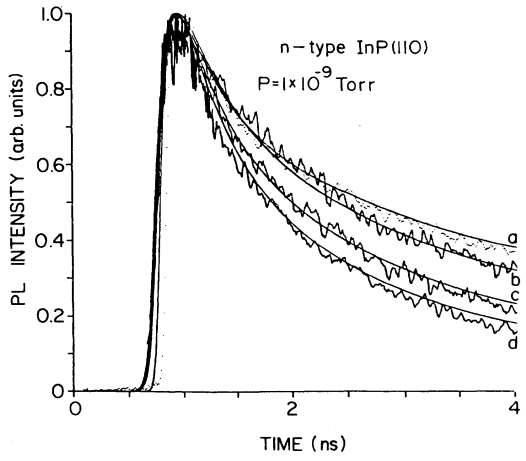

FIG. 18. Experimental and calculated (solid curves) photoluminescence decay curves for cleaved n-type InP (110) under a pressure of 1×10^{-9} Torr, measured using the diode laser. b, as cleaved ($v_{SR}=5\times10^3$ cm/s); c, after 45 min ($v_{SR}=1.4\times10^4$ cm/s); d, after 90 min ($v_{Sr}=3.0\times10^4$ cm/s). a, the etched surface decay curve is shown for comparison.

If, for simplicity, we assume that the cross section for electron-hole recombination σ is equal to 1×10^{-15} cm^2, we obtain

$$N_s=(S_0-S_0^*)/\sigma V_{\rm th}\simeq 5\times10^{11}\ {\rm cm}^{-2}\ ,$$

where S_0^* is the SRV of the freshly cleaved sample. This very simplistic calculation demonstrates the great sensitivity of our time-resolved PL technique. Examination of Fig. 18 shows that the sensitivity can be easily improved, since much smaller changes in SRV values can be detected. Steady-state PL is commonly used for quality evaluation of crystal surfaces, despite its disadvantage of being a relative measurement. Also, the steady-state PL may change due to factors other than SRV (mainly the bulk lifetime). Our technique makes it possible to discriminate between surface and bulk recombination, as was described in detail in the paper. Time-resolve PL can be also used as a tool for estimating cleavage quality and surface cleanliness critical for UHV studies. For example, in the field of metal-semiconductor interfaces it is crucial to know whether the semiconductor surface is free of sub-band-gap states prior to metal evaporation. This is usually done by XPS even though it is capable of detecting surface states only at concentrations above $\sim1\times10^{12}$ cm^{-2}. Our results show that the time-resolved PL technique may be superior for this purpose.

Besides its lower SRV, the etched InP(110) surface is also more stable than the cleaved surface (see Sec. IV A). The reason may be a passivating oxide layer which is formed on the crystal surface as a result of the etching process. Surface studies[33] report of a 5–20-Å-thick oxide layer that grows rapidly on the InP surface after aqua regia etching. However, etched surfaces did not retain the low SRV after baking the UHV system or exposure to hot filaments.

V. SUMMARY AND CONCLUSIONS

We have presented a detailed time-resolved PL study of the InP crystal. Our results highlight the strength of this technique in obtaining important information about surface- and bulk-recombination processes in semiconductors. It was found that aqua regia–etched n-type InP(110) has low intrinsic SRV (200 cm/s) and large τ (320 ns). p-type InP has similarly low intrinsic SRV (500 cm/s) but, on the other hand, much smaller $\tau(\leq 33$ ns). We have shown that this τ is probably due to deep traps which have greater cross section for electron-hole recombination. Thus, $\tau_{\rm nr}$ in p-type InP is much smaller than τ_r and the nonradiative recombination process is dominant. In n-type InP $\tau_{\rm nr}$ is very large (around 300 ns) and thus the bulk recombination is mainly radiative. These conclusions are based on the different dependences of the bulk lifetime on the excess-carrier concentration in the two types of InP. We have also shown that the low luminescence efficiency of p-type InP is due to its low lifetime and to the large band bending at the surface.

Our results for (n-type InP)/metal interfaces have shown that SRV has a distinct dependence on the reactivity of the metal-semiconductor pair. This dependence is similar to the dependence of the Schottky-barrier height on ΔH_R, and thus has important consequences for current studies of metal-InP interfaces. Measurements conducted under UHV conditions have shown that the SRV of cleaved n-type InP(110) is greater than at aqua regia–etched surfaces.

ACKNOWLEDGMENTS

This research was supported in part by Grant No. 266/89 from the basic research foundation of the Israeli Academy of Sciences and Humanities and by a grant from the James Frank Binational German/Israeli program in laser-matter interaction.

[1]V. Diadiuk, S. H. Grove, C. E. Hurwitz, and G. W. Iseler, IEEE J. Quantum Electron **QE-17**, 260 (1981).
[2]S. R. Forrest, G. F. Williams, O. K. Kim, and R. G. Smith, Electron. Lett. **17**, 917 (1981).
[3]L. Messick, D. A. Collins and D. L. Lile, IEEE Electron Device Lett. **7**, 680 (1986).
[4]M. W. Wanlass, T. J. Coutts, J. S. Ward, K. A. Emery, and G. S. Horner, *Third International Conference on InP and Related Materials, Wales,* edited by T. Riley (IEEE, New York, 1991).
[5]R. K. Ahrenkiel, in *Properties of InP* (INSPEC, London, 1991), p. 77.
[6]R. K. Ahrenkiel, D. J. Dunlavy, and T. Hanak, J. Appl. Phys. **64**, 1916 (1988).
[7]H. C. Casey, Jr. and E. Buehler, Appl. Phys. Lett. **30**, 247 (1977).
[8]C. A. Hoffman, H. J. Gerritsen, and A. V. Nurmikko, J. Appl. Phys. **51**, 1603 (1978).
[9]S. Bothra, S. D. Tyagi, S. K. Ghandhi, and J. M. Borrego, *Proceedings of the 21st Photovoltaic Specialists Conference,* edited by IEEE (IEEE, New York, 1990).
[10]M. Evenor, S. Gottesfield, Z. Harzion, D. Huppert, and S. W. Feldberg, J. Phys. Chem. **88**, 6213 (1984).
[11]Y. Resnewaks, L. Burstein, Y. Shapira, and D. Huppert, J. Phys. Chem. **94**, 6842 (1990); Appl. Phys. Lett. **57**, 458 (1990).
[12]P. Besler-Podorowsky, D. Huppert, Y. Rosenwaks, and Y. Shapira, J. Phys. Chem. **95**, 4370 (1991).
[13]Y. Rosenwaks, Y. Shapira, and D. Huppert, Appl. Phys. Lett. **57**, 2552 (1990); Phys. Rev. B **44**, 13 097 (1991).
[14]A. Many, Y. Goldstein, and N. G. Grover, *Semiconductor Surfaces* (North Holland, Amsterdam, 1965).
[15]J. Vaitkus, Phys. Status Solidi A **34**, 769 (1976).
[16]A. V. Rzhanov and I. A. Arkhipora, Fiz. Tver. Tela (Leningrad) **3**, 1954 (1962) [Sov. Phys. Solid State, **3**, 1424 (1962)].
[17]H. C. Casey, Jr. and F. Stein, J. Appl. Phys. **47**, 631 (1976).

[18]P. Asbeck, J. Appl. Phys. **48**, 820 (1977).
[19]D. E. Aspnes, Surf. Sci **132**, 406 (1983).
[20]D. B. Wittry and D. F. Kyser, J. Appl. Phys. **38**, 375 (1967).
[21]K. Ando, A. Yamamoto, and M. Yamaguchi, Jpn. J. Appl. Phys. **20**, 1107 (1981).
[22]A. S. Grove, *Physics and Technology of Semiconductor Devices* (Wiley, New York, 1967).
[23]R. H. Williams and I. T. McGovern, Surf. Sci. **51**, 14 (1975).
[24]W. Shockley and W. T. Read, Jr. Phys. Rev. **87**, 835 (1952).
[25]*Lange's Handbook of Chemistry,* edited by J. A. Dean (McGraw-Hill, New York, 1973).
[26]N. Convers Wyeth and A. Catalano, J. Appl. Phys. **51**, 2286 (1980).
[27]R. H. Williams, R. R. Varma, and V. Montgomery, J. Vac. Sci. Technol. **16**, 1418 (1979).
[28]E. Hökelek and G. Y. Robinson, Appl. Phys. Lett. **40**, 426 (1982).
[29]L. J. Brillson, C. F. Brucker, A. D. Katnani, N. G. Stoffel, R. Daniels, and G. Margaritondo, J. Vac. Sci. Technol. **21**, 564 (1982).
[30]O. J. Glenbocki, H. Piller, in *Handbook of Optical Constants of Solids,* edited by E. D. Palila (Academic, London, 1985), p. 503.
[31]R. J. Nelson, Rev. Sci. Instrum, **49**, 770 (1978).
[32]T. A. Louis, Rev. Sci. Instrum. **61**, 11 (1990).
[33]D. E. Aspnes and A. A. Studna, Appl. Phys. Lett. **39**, 316 (1981).